Supplementary Materials

Enhanced thermal management performance of nanofibrillated cellulose composite with high thermal conductive boron phosphide

Jiajun Hu,[†] Hongyan Xia[*,†], Xinguang Hou,[†] Ting Yang,[†] Kang Si, [†] Yi Wang,[†] Laili Wang[‡], Zhongqi Shi[*,†]

[†]State Key Laboratory for Mechanical Behavior of Materials, Xi'an Jiaotong University, Xi'an 710049, China

[‡]School of Electrical Engineering, Xi'an Jiaotong University, Xi'an 710049, China

[*]Corresponding authors.

E-mail addresses: hyxia0707@xjtu.edu.cn (Hongyan Xia), zhongqishi@mail.xjtu.edu.cn (Zhongqi Shi).

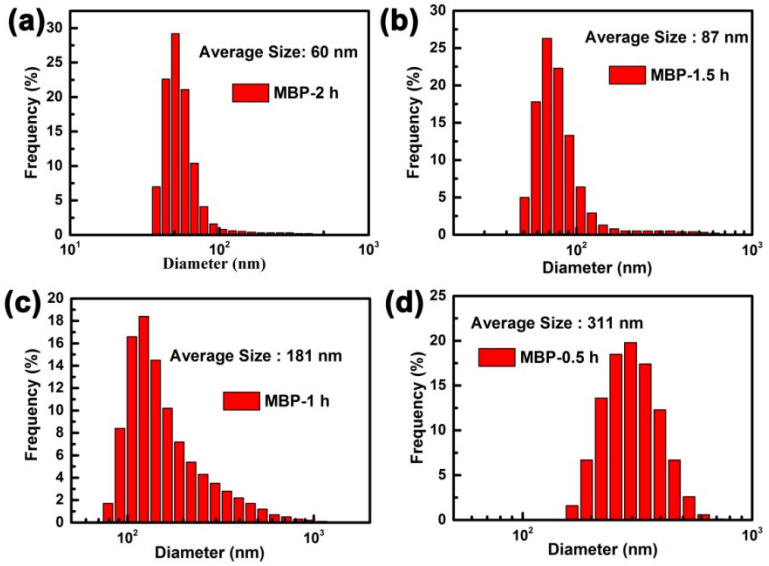

Figure S1. Size distribution of MBP particles with ball milling time of (a)2 h; (b)1.5 h; (c) 1 h; (d) 0.5 h.

.

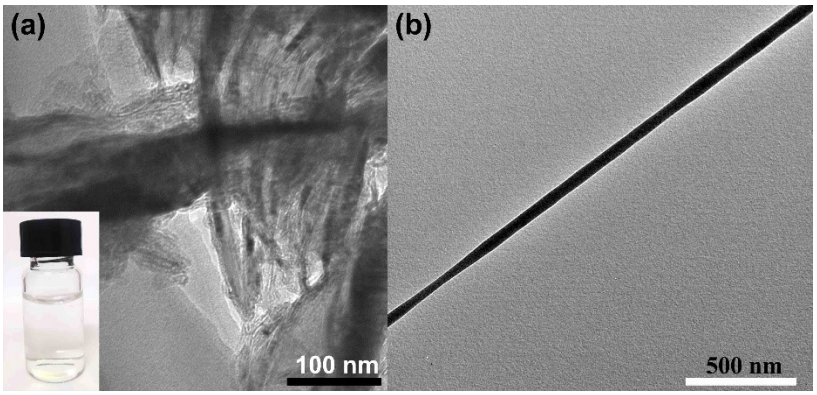

Figure S2. TEM image of (a) NFC aggregates and (b) single NFC. The inset in (a) was the optical photo of NFC solution.

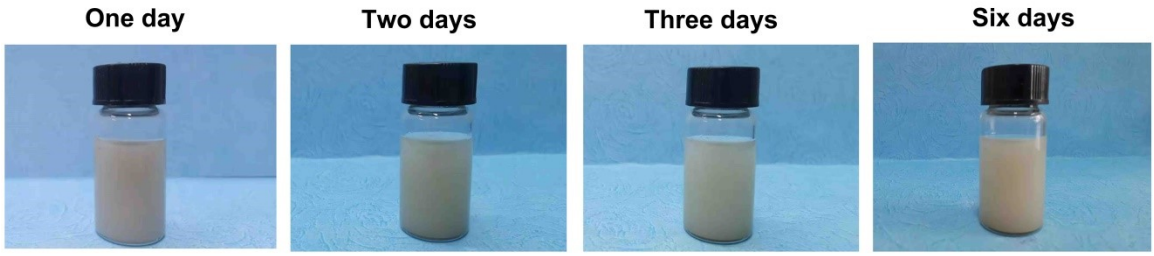

Figure S3. Optical images of NFC/MBP15 suspension at different days. Here MBP was ball milled with the time of 2 h.

Figure S4. Optical image of NFC/MBP suspension showing “Dyndall effect”.

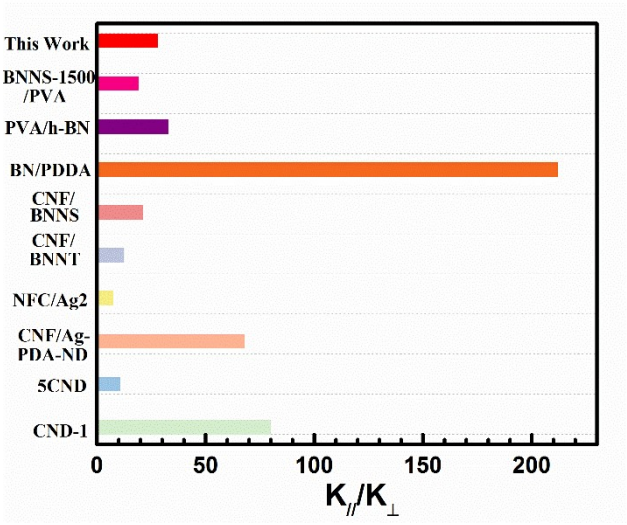

Figure S5 Comparison of the anisotropic value of NFC/MBP composites film with some reports [1-8].

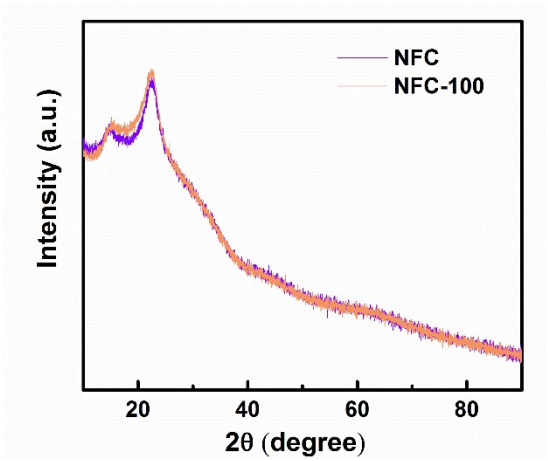

Figrue S6. XRD patterns of NFC and NFC-100. NFC film was heat treated at 100 ℃ for NFC-100.

Theoretical approach to analyzing experiment data:

In this work, the addition of MBP improved the thermal conductivity of NFC/MBP15 composite films obviously. To understand the heat transfer mechanism of the composite films, the effective medium theory (EMT) was used to predict the thermal conductivity of composite films and calculate the interface thermal interface between the MBP and NFC. In EMT model, when the MBP filler was

considered as sphere, and it was used to fit the thermal conductivity of NFC/MBP15 composite films as following:

Type 1: Spheres

When the MBP particles were considered as sphere, p=1, L_{11}=L_{33}=1/3, γ=(1+2p)α=3α and $\langle \cos^2\theta \rangle$=1/3. Then the equation K_{ii}^{c}= K_p/(1+$\gamma L_{ii} K_p/K_m$) was simplified to K_{11}^{c}= K_{22}^{c}= K_{33}^{c} =K_p/(1+$\alpha K_p/K_m$). Finally, on the basis of these value, K value was fitted by the following equation to obtain the interface thermal resistance (R_i) between the filler and matrix.

$$K = K_m \frac{K_p(1+2\alpha) + 2K_m + 2f[K_p(1-\alpha) - K_m]}{K_p(1+2\alpha) + 2K_m - 2f[K_p(1-\alpha) - K_m]} \quad \text{(S1)}$$

$$\alpha = \frac{R_i K_m}{a_3} \quad \text{(S2)}$$

The fitting results were shown in Figure S7, it was obviously that the fitting curve did not match the thermal conductivity value of NFC/MBP15 composite films. Therefore, the spherical hypothesis model was not suitable for this work.

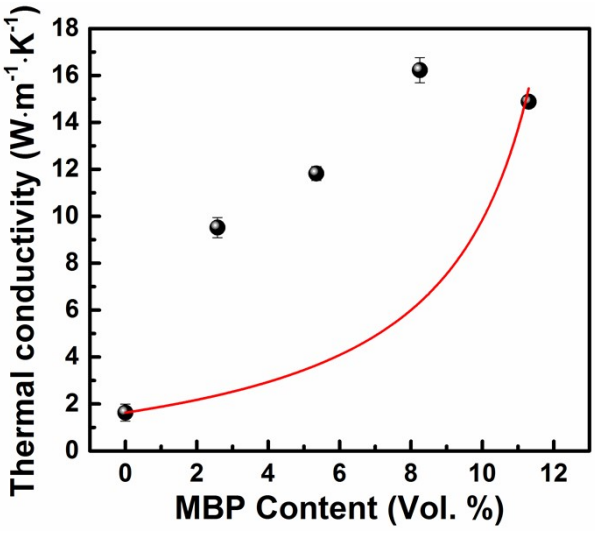

Figure S7. Spherical hypothesis model fitting curves for the thermal conductivity value of

NFC/MBP15 composite films.

The thermal conduction behavior of pure NFC, randomly dispersed NFC/MBP15 and NFC/MBP15 composite films were modeled by computational fluid dynamics software (COMSOL Multiphysics 5.4). In the model simulation, the thermal conductivity of MBP was set to 250 W m^{-1} K^{-1}. The dimension of three cases was set to be 600×600×600 nm with spherical MBP filler of 60 nm in diameter. Considering that the volume fraction of MBP in the models of NFC/MBP15 and randomly dispersed NFC/MBP15 was 8.25%, there were 160 dispersed MBP spheres in the two models, respectively. As shown in Figure S8, for NFC/MBP15 model, according to the cross-sectional SEM images of NFC/MBP15 composite film, it was assumed that some MBP particles were connected to form short-range and ordered arrangement and distributed in NFC matrix evenly. The composite film was contacted with the bottom surface of heat source (100×100×100 nm) with a tem1perature of 100 ℃. Except for the area contacted with heat source, the other outer boundaries had no heat excha

nge with external environment. In addition, the whole time length of the three models were 10 ns with a step length of 1 ns.

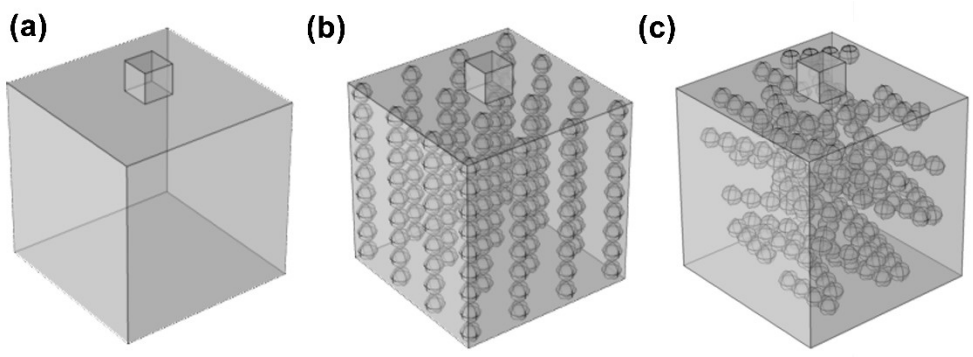

Figure S8. The finite element models of (a) pure NFC; (b) randomly dispersed NFC/MBP15 and (c) NFC/MBP15 films in this work.

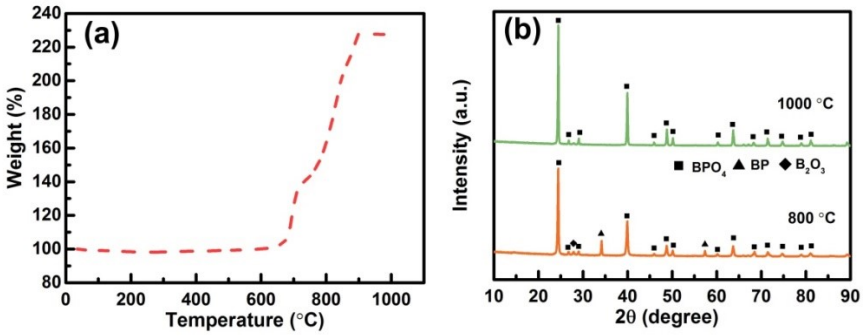

Figure S9. (a) Thermogravimetric curve of BP in air; (b) XRD patterns of the oxidation of BP at different temperature.

Table S1. The detailed parameters and results of NFC/MBP composite films for thermal conductivity.

Sample	ρ ($g \cdot cm^{-3}$)	C_p ($J \cdot g^{-1} \cdot K^{-1}$)	$D_{//}$ ($mm^2 \cdot s^{-1}$)	$D_{\perp}$ ($mm^2 \cdot s^{-1}$)	$\lambda_{//}$ ($W \cdot m^{-1} \cdot K^{-1}$)	$\lambda_{\perp}$ ($W \cdot m^{-1} \cdot K^{-1}$)
Pure NFC	1.480	1.460	0.754	0.100	1.630	0.216
NMB5	1.530	1.440	4.262	0.319	9.390	0.704
NMB10	1.550	1.424	5.200	0.347	11.470	0.767
NMB15	1.576	1.405	7.270	0.360	16.090	0.798
NMB20	1.599	1.385	6.709	0.356	14.850	0.788

Table S2 The thermal conductivity parameters of finite element models

Sample	In-plane Thermal conductivity/ $W\ m^{-1}\ K^{-1}$	Through-plane thermal conductivity/ $W\ m^{-1}\ K^{-1}$
NFC	1.63	0.216

References

[1] S.D. Yang, X. Sun, J.Q. Shen, Y. Li, L. Xie, S.H. Qin, B. Xue and Q. Zheng, Interface Engineering Based on Polydopamine-Assisted Metallization in Highly Thermal Conductive Cellulose/

Nanodiamonds Composite Paper, *ACS Sustainable Chem. Eng.*, 2020, **8**, 17639−17650.

[2] Z.M. Shen and J.C. Feng, Highly Thermally Conductive Composite Films Based on Nanofibrillated Cellulose in Situ Coated with a Small Amount of Silver Nanoparticles, *ACS Appl. Mater. Interfaces*, 2018, **10**, 24193-24200.

[3] K. Wu, J.C. Fang, J.R. Ma, R. Huang, S.G. Chai, F. Chen and Q. Fu, Achieving a Collapsible, Strong, and Highly Thermally Conductive Film Based on Oriented Functionalized Boron Nitride Nanosheets and Cellulose Nanofiber, *ACS Appl. Mater. Interfaces*, 2017, **9**, 30035-30045.

[4] X.L. Zeng, J.J. Sun, Y.M. Yao, R. Sun, J.B. Xu and C.P. Wong, A Combination of Boron Nitride Nanotubes and Cellulose Nanofibers for the Preparation of a Nanocomposite with High Thermal Conductivity, *ACS Nano*, 2017, **11**, 5167-5178.

[5] Y.P Wu, Y. Xue, S. Qin, D. Liu, X.B. Wang, X. Hu, J.L. Li, X.G. Wang, Y. Bando, D. Golberg, Y. Chen, Y. Gogotsi, and W.W. Lei, BN Nanosheet/Polymer Films with Highly Anisotropic Thermal Conductivity for Thermal Management Applications, ACS Appl. Mater. Interfaces, ACS Appl. Mater. Interfaces, 2017, **9**, 43163-43170.

[6] O.H. Kwon, T. Ha, D.G. Kim, B.G. Kim, Y.S. Kim, T.J. Shin, W.G. Koh, H.S. Lim, and Y. Yoo, Anisotropy-Driven High Thermal Conductivity in Stretchable Poly(vinyl alcohol)/Hexagonal Boron Nitride Nanohybrid Films, *ACS Appl. Mater. Interfaces*, 2018, **10**, 34625−34633.

[7] Q.W. Yan, W. Dai, J.Y. Gao, X. Tan, L. Lv, J.F. Ying, X.X. Lu, J.B. Lu, Y.G. Yao, Q.P. Wei, R. Sun, J.H. Yu, N. Jiang, D. Chen, C.P. Wong, R. Xiang, S. Maruyama, and C.T. Lin, Ultrahigh-Aspect-Ratio Boron Nitride Nanosheets Leading to Superhigh In-Plane Thermal Conductivity of Foldable

Heat Spreader, *ACS Nano*, 2021, **15**, 6489−6498.

[8] N. Song, D.L. Cao, X. Luo, Y.Q. Guo, J.W Gu and P. Ding, Aligned cellulose/nanodiamond plastics with high thermal conductivity, *J. Mater. Chem. C*, 2018, **6**, 13108—13113.